

Challenges in metrology of bio-mimicking microphantoms for quantitative phase imaging: perspective

Michał Ziemczonok

Warsaw University of Technology, Institute of Micromechanics and Photonics

Dariusz Czudek

Central Office of Measures, Time and Length Department

Małgorzata Kujawińska

Warsaw University of Technology, Institute of Micromechanics and Photonics

Corresponding author's e-mail address: michal.ziemczonok@pw.edu.pl

Abstract

Quantitative Phase Imaging (QPI) refers to 2D and 3D microscopy techniques that provide contrast by quantifying the phase changes in the wavefront when light propagates through specimen. The QPI is particularly useful as advanced imaging and measurement tool in biomedical research, but its performance is sample-dependent and cannot be reliably characterized with conventional approach to metrology. In order to benchmark the QPI system it is crucial to use phantoms that represent key details of the sample in realistic working conditions, and evaluate the system in an end-to-end fashion. This work summarizes the metrological needs for the QPI, as well as presents 3D-printed phantoms ranging from simple bars, steps, cells and cell cultures, up to volumetric and scattering phantoms mimicking tissues or organoids. If such phantoms could be characterized by traceable and calibrated instruments, they would become invaluable tool to certify QPI instruments and enable reliable measurement outcomes.

Keywords: Optical metrology; Quantitative phase imaging; Imaging phantoms; Two-photon polymerization; Biomedical imaging.

1. Introduction

Quantitative Phase Imaging (QPI) refers to a number of label-free 2D and 3D microscopy techniques that provide contrast by quantifying the phase changes in the wavefront when light propagates through transparent specimen [1, 2]. QPI provides means for measurement and imaging of biological or technical microstructures, merging beneficial features of microscopy, phase measurement methods (including interferometry and holography), and numerical (2D and 3D) computations. In biomedical applications, 2D QPI (phase microscopy) numerically converts recorded interference pattern into a map of optical delay [3–5], also called optical path difference (OPD) or an integrated phase of a sample (Fig. 1a), often with nanoscale resolution and precision. The retrieved OPD is obtained as:

$$OPD(x, y) = d(x, y) \cdot n(x, y) \quad (1)$$

where $d(x,y)$ is the thickness of a sample and $n(x,y)$ is the average refractive index (RI) along the considered height. OPD can also be expressed as

$$\phi(x, y) = OPD(x, y) \cdot \frac{2\pi}{\lambda} \quad (2)$$

where ϕ is the phase delay of the light with a given wavelength λ . This approach provides contrast even in optically transparent objects, such as biological cells (Fig. 1b). Furthermore, the OPD map enables to segment cells within

monolayer cell culture and calculate their biophysical properties such as dry mass, area and motility [6] in order to study e.g. immune cell behavior [7], neuron dynamics [8] and advance precision cancer medicine [9]. In 3D QPI systems tomographic reconstruction is based on a series of images captured as multiple angular projections of a sample (Fig. 1c). Then, the 3D RI is obtained analytically from the synthesized 3D scattering potential under Fourier Diffraction Theorem [10, 11], or using various optimization solvers that iteratively solve for sample's 3D RI by minimizing the error between measured and numerically propagated intensities or complex amplitude fields [12–14]. Machine learning is also being explored to perform tomographic reconstruction using physics-informed neural networks [15–17]. 3D QPI is applied to study more relevant, three-dimensional biological objects such as tissue slices [18], spheroids [13], organoids [19] and even entire organisms [12, 20] to reveal their morphology, analyze growth or detect pathological states.

The measurement process in 2D and 3D QPI is non-invasive and label free, meeting the demand for advanced imaging technologies in biomedical research. Several [2] research and commercial QPI systems are available [2] covering a wide range of magnifications, spatial resolutions, accuracies and functionalities. Performance of QPI instruments depends on optical system parameters (numerical aperture, scanning, noise), light propagation modelling (e.g. scattering, coherence) and data processing [21] (demodulation, tomographic reconstruction), creating unique challenges for their metrology.

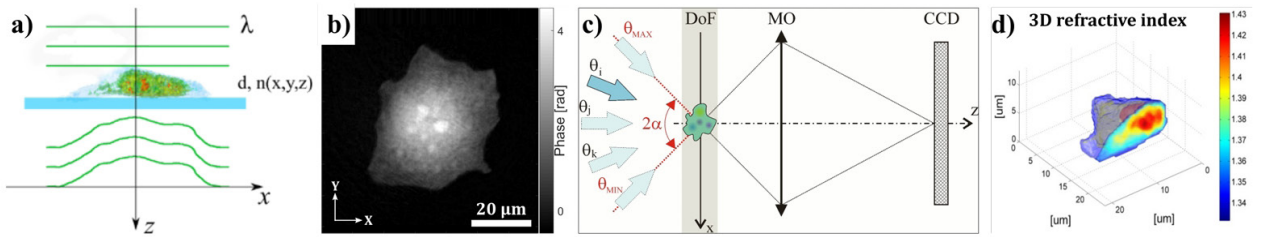


Fig. 1. The principle of QPI measurements: 2D QPI and example result of a 2D integrated phase (a-b) and 3D QPI and example result of a 3D refractive index distribution (c-d), of a biological cell. DoF- depth of focus, MO- microscope objective, CCD-camera sensor.

Apart from system performance itself, the utility of full-field phase measurement in biomedical applications also depends on the sample complexity and result analysis algorithms. This creates a lot of uncontrolled degrees of freedom and the interplay between these factors cannot be reliably measured. Instead, in order to evaluate the system it is crucial to use phantoms that represent key details of the sample and therefore can provide a benchmark for calibration and validation of QPI systems in realistic

working conditions, enabling end-to-end approach to metrology.

Currently available 2D QPI test targets are inadequate, because: (1) they contain purely geometrical shapes and their phase value is constant within those regions; (2) optical path difference is introduced between the substrate (usually glass) and air, which yields refractive index contrast of about 0.5. Therefore the current solutions cannot represent real samples for which 2D QPI

systems are optimized for, that is biological cell and cell cultures measurements. The phase range and variability should correspond to the biological cells. The refractive index contrast between the sample and the background should be around 0.03 in order to land within typical values of phase, height and refractive index of the measured objects. Moreover, commercially available targets are typically made of materials and substrates required by the applied manufacturing process, which are different than cover glasses or Petri dishes used to image biological samples. Due to different imaging conditions and additional optical aberrations, the results obtained from such targets cannot be directly transferred to biological experiments. Similarly in 3D, the resolution test charts or microbeads are commonly used to evaluate the tomographic reconstructions with at least geometrical traceability, however commercially offered targets are too simple and lack the typical biological diversity and RI entropy seen in complex biological samples.

Considering the lack of test targets for 2D and 3D QPI that can mimic phase and RI profiles of biological microstructures the works have begun on the design of such standards and the search for methods for their production. Two-photon polymerization (TPP) has been shown to address all main challenges for phantom fabrication outlined above, that is geometry, RI contrast and sample compatibility [21, 22]. TPP utilizes tightly focused femtosecond laser beam to locally solidify photosensitive resin using the

principles of two-photon absorption [23, 24]. The microstructures emerge as the beam focus is scanned across the liquid resin in line by line, layer by layer fashion featuring submicrometer resolution in all three dimensions [25]. The degree of monomer cross-linking depends on the energy dose [26], which can be exploited to engineer the refractive index distribution within the processed volume. As a result, TPP enables fabrication of transparent, structurally complex samples with submicrometer features and predetermined 3D RI distribution [27]. However, the measurement traceability of these phantoms decline, as most metrological protocols and guidelines are suitable only for well-defined height profiles [28, 29]. Here we provide an overview of the crucial parameters for evaluation in the QPI systems, the corresponding test targets that are feasible for fabrication using TPP, as well as we summarize the challenges related to metrology of said structures and QPI systems.

2. Measurement range and fabrication considerations

The 2D and 3D QPI provide exceptional accuracy and throughput, combining high resolution at relatively large field of view and captured rapidly when compared to tactile/linear scanners. Typical range of accessible parameters has been summarized in Tab. 2, along with the corresponding parameters of the 3D-printing via TPP.

| Feature | 2D QPI | 3D QPI | TPP |
|----------------------------------|-----------|-------------|-------------|
| Size (μm) | 0.3–3 000 | 0.15–200 | 0.1–10 000 |
| Phase (rad) | 0.01–10 | — | 0.01–50 000 |
| Refractive index | — | 0.0001–0.05 | 0.001–0.5 |
| Measurement/fabrication time (s) | 0.03 | 2 | 60–100 000 |

Table 1. Range of key parameters of the QPI systems and the TPP technique.

In case of the QPI, lower limit of size or phase/RI corresponds to the spatial resolution and sensitivity of the instrument, while the upper limit is related to the field of view and measurement range, respectively. While the whole range of indicated parameters is rarely utilized in a single instrument, it is in principle possible using various stitching or multiplexing approaches. The upper limit of phase and RI can differ significantly between different implementations of QPI, but generally a few wavelengths of phase shift in weakly scattering samples (RI contrast within 0.05) is considered satisfactory. Beyond that the errors are rapidly increasing and specialized hardware and software solutions are required. In biomedical applications the range of measurand is fundamentally imposed by the

sample and biological problem at hand, therefore expanding this range is of great importance to enable QPI of thick tissue slices, organoids or even entire microorganisms.

TPP covers the required parameters range in all but one aspect, that is lower bound of RI. In conjunction with the ability to address main challenges outlined in the Introduction, the TPP reinforces its position as the suitable method for phantom fabrication. While the RI range accessible within a single resin is relatively small (at the order of 0.03, the difference between monomer and fully polymerized states), this is close to the range of values represented in biological specimens. However, the RI range can be easily extended up to 0.5 using multiple materials

[24] or immersing the sample in the RI-calibrated medium of choice.

Fabrication time indicated in the table is related to the scan speed and laser power available in the system, as well as the structure's fidelity and printed volume. Structures mimicking single cells could take a minute to fabricate, while e.g. organoids typically take about an hour, on top of the 15 mins needed for the development. Longer prints, that is at high resolution and/or volume can take over a day and drive up the cost, but this doesn't have negative impact on the utility. In case of the QPI however, the measurement time is related to noise characteristics and, more importantly, temporal resolution. Minimization of measurement time is critical in imaging of live specimens due to dynamic processes. 2D QPI generally requires a single image and is limited by the exposure time and/or frame rate of the camera, while 3D QPI relies on tens or hundreds of images to reconstruct the 3D RI. Especially in 3D QPI motion blur might be the reason behind discrepancy of the resolution determined in the stationary phantom and in e.g. living cells. Longer acquisition times, however, could be beneficial to increase sensitivity via averaging.

3. 3D-printed microphantoms for QPI

In this section various test structures for QPI ranging from simple marks and bars, steps, cells and cell cultures, up to volumetric and scattering phantoms mimicking tissues or organoids are presented.

3.1 One-dimensional

Spatial resolution and image magnification of QPI system are crucial to determine the minimal feature size that can be resolved, as well as the proper lateral scaling of the acquired images that contribute to the area and dry mass measurement accuracy. In general, the commercial targets for resolution and magnification are widely available in both amplitude and phase variants [30, 31]. The structures made using TPP are designed to be measured at appropriate RI contrast, which makes the measurement conditions quite different than targets measured in air. If commonly used air targets (typically within 100–500 nm in height) are used in a low contrast setting, then the phase signal is weak and the resolution reading is heavily impacted by the precision or signal-to-noise of the instrument. If the height is increased to match the phase magnitude of the biological samples, the target may exceed the depth of focus, in which case the wavefront does not represent integrated phase due to light diffraction. These major differences arising from RI contrast of the measured sample contribute to the measurement outcomes even when using simple geometry targets, and have to be considered when designing targets and benchmarking new instruments.

The resolution targets could be used to evaluate the instrument transfer function [32], which ties amplification coefficient (in this case phase/RI response) to the spatial frequency, providing more comprehensive way to characterize the system. This response can differ depending on direction, field of view and the proportion between height and RI contrast contribution to the measured phase, so still more guidelines are needed to standardize even resolution evaluation in QPI.

In the case of magnification, it is feasible to provide traceability. Required accuracy depends on the pixel size of the camera and magnification of the optical system. For the current most demanding QPI systems uncertainty requirement for the magnification target positions is around 40 nm over 120 μm field of view (0.03%), so that the magnification error below that value would scale the whole image by no more than half a pixel.

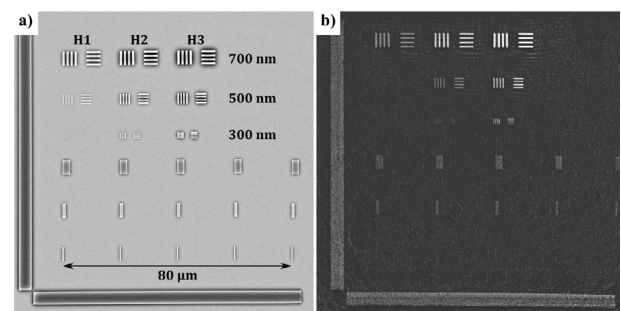


Fig. 2. Scanning electron microscopy (a) and QPI (b) image of the TPP test structures for determination of resolution (300–700 nm line width, with increasing heights H1-H3) and magnification.

3.2 Two-dimensional

2D phase maps constitute the main output of the full-field QPI system, where the optical path delay is evaluated at each pixel. Since biological specimen variability is extremely high (cells of different types, tissue of various organs etc.), it is impractical to benchmark the performance using material measures, such as described in ISO 5436-1 or ISO 25178, if the measurement system is sample-dependent with tightly integrated reconstruction and processing software. For this reason, 3D-printed phantoms can be obtained by recreating the height map that corresponds to the phase measurements of the actual biological samples [33]. Such phantom mimics the features that are of interest for biomedicine, while also enabling the benchmarking using feature vectors consistent with analysis pipeline appropriate for the particular imaging task. Nevertheless both types of structures, that is technical and biomimicking, can be fabricated on a single substrate (Fig. 3), bridging the gap between standardized artifacts and lifelike phantoms.

The issue with metrological traceability of such phantoms arises since there are two critical variables to validate: height and RI. In typical calibration artifacts used in reflection mode the RI of air can be accurately calculated in a controlled environment, and therefore its error contribution is usually negligible. In the case of 3D-printed structures intended to be measured in physiological conditions (low-RI contrast) in transmission, the considered RI contrast is between the RI of a 3D-printed polymer and the RI of an immersion liquid. Even though the immersion liquids can be measured quite accurately (off-the-shelf certified liquids can have the RI uncertainty at the order of 0.0002), the accurate measurement of the RI of the polymer is still a challenge. Methods based on total internal reflection require large volumes of TPP material and the surface of the polymer could have different parameters than the bulk material due to resin chemistry and proximity effects, rendering reflection methods for RI measurement unsuitable.

Even though the 2D systems provide integrated phase, the phantom has to be characterized in terms of its height and RI in order to incorporate correction factors such as chromatic dispersion or temperature coefficient. In principle the most suitable methods for accurate polymer RI

determination would be calibrated QPI system that provide phase measurements, which can be combined with traceable height measurement. An alternative approach would be to measure phase shift in two certified RI immersion liquids, which require additional sample preparation and cleaning. Step structure with regions representing two distinct optical path values are necessary, such as shown in the Fig. 3d). The problem is, that the calibrated systems typically work in reflection and with micrometer-thin samples as outlined in the Introduction, making them unsuitable for measurements of relatively tall structures ($\sim 20 \mu\text{m}$). Additionally, this approach can introduce circular problem where optical method akin to QPI is used to characterize the RI, which is then intended to be used for QPI validation. Lack of other techniques that could provide direct reference for QPI measurements in the case of cell phantoms, where high accuracy, resolution and field of view is required simultaneously pose a great challenge for 2D QPI metrology.

3.3 Three-dimensional

Phantoms for 3D QPI require exceptionally high spatial resolution (up to 150 nm), as well as controlled three-dimensional RI distribution. Both features are enabled by

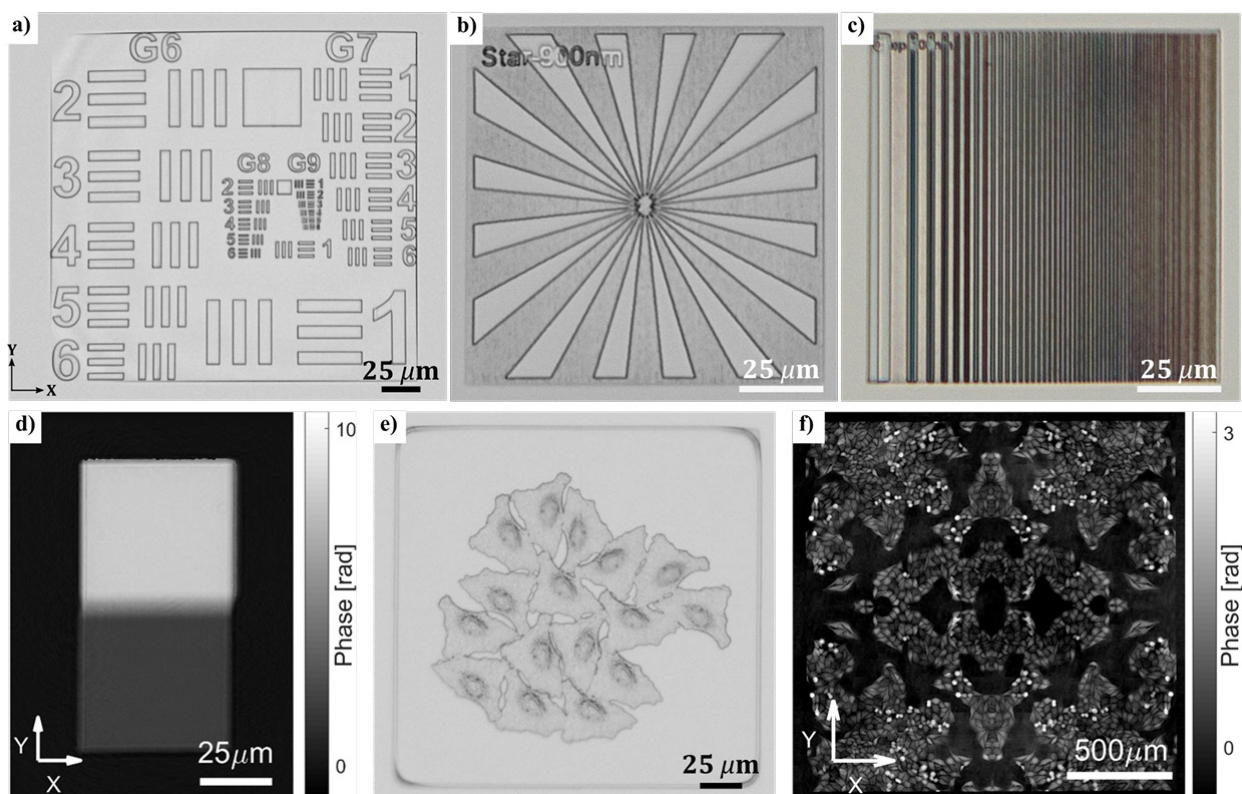


Fig. 3. An assortment of 3D-printed test structures useful for evaluation of 2D QPI: a) bright-field microscope image of a USAF resolution test chart (groups 6-9), b) spoke target, c) chirp target (color gradient indicate interference filtering artifacts), d) phase image of the step structure, e) bright-field image of the cell phantom arranged in high-confluence sample, f) phase image of a 2.5 mm² cell culture phantom stitched from 15x15 fields of view.

the TPP, where the gradual degree of conversion of the resin from monomer to polymer change local density and thus refractive index. This enables fabrication of phantoms that very well mimic the optical properties of biological specimens in the context of QPI.

Artificially designed phantoms are advantageous because of their well-defined features, such as resolution cuboids or ellipsoidal inclusions, that are straightforward to quantify and compare. The example of the phantom of a single cell is shown in Fig. 4a. It has been used to directly compare and learn from the results obtained from three 3D QPI systems [21]. Extending this idea, it is possible to create an array of artificial cells in the form of a monolayer (Fig. 4b) or a 3D cell cluster, which mimic the most common biological arrangements. Cell phantom can also be embedded inside of another microstructure that increase the

difficulty of imaging by e.g. exhibiting adjustable scattering properties of a tissue [34] (Fig. 4b-c). Finally, the TPP can recreate arbitrary RI distribution designed artificially (Fig. 4d-e) or coming directly from measurements of a real sample, capturing the RI entropy of complex biological specimens such as organoids (Fig. 4f-g). These initial measurements used as a basis for the phantoms are obviously erroneous with respect to the true morphology of the specimen, however, with the continuous advancements in both 3D QPI and TPP it is envisioned that these techniques can feed into each other and enable more and more accurate measurements, that become more and more accurate phantoms. Finally, this approach aims at providing both physical phantoms and digital twins of specific groups of biological microobjects.

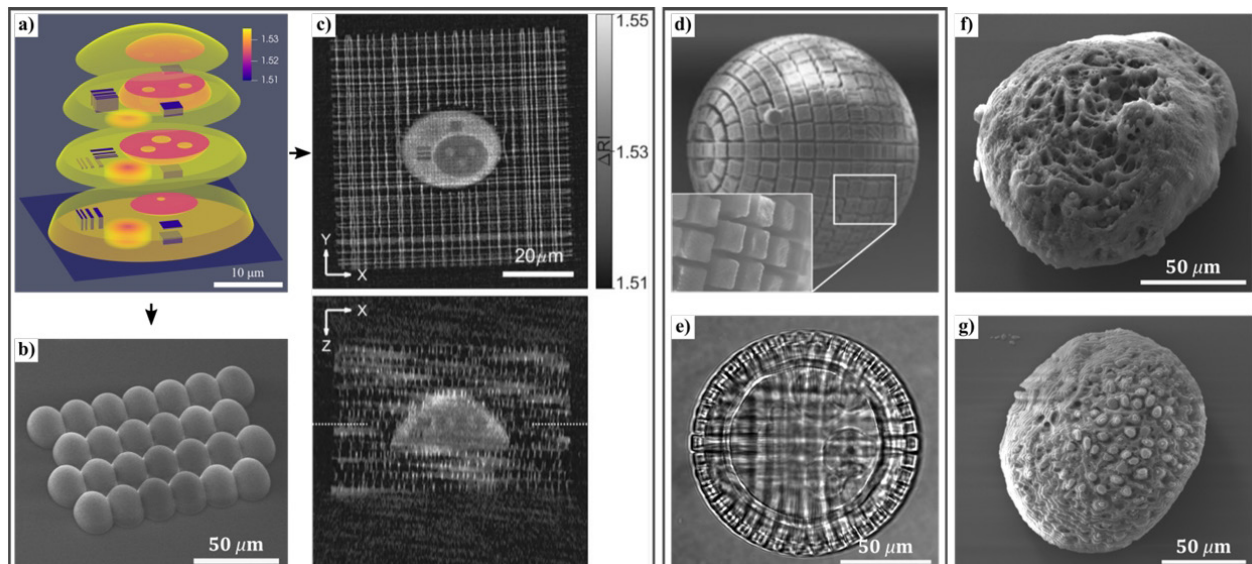


Fig. 4. An assortment of 3D-printed test structures useful for evaluation of 3D QPI: a) single cell phantom with intracellular compartments and refractive index contrast, b) scanning electron microscopy image of an array of single cell phantoms from a) arranged in a monolayer, c) 3D QPI measurement of the cell phantom from a) embedded into the porous cube (fabricated simultaneously) to increase the scattering of light, d-e) artificially designed 3D cell cluster with scattering cubes on the surface, captured by the scanning electron microscope and brightfield microscope, f-g) scanning electron microscopy image of the organoid phantoms, that were designed using measurements of real organoids.

Metrological challenges in 3D QPI stem from stability of the structure, as well as complete lack of appropriate reference measurement methods. The first limitation is related to the fact, that partially-polymerized resin exhibit low mechanical stability and such regions of the phantom can excessively shrink, are vulnerable to solvents and photosensitive. Therefore the design, handling and storage of such phantoms to ensure their key metrological parameters is challenging. The second limitation relates to the wealth of information provided by the 3D QPI, that is fully volumetric data at high spatial resolution and RI accuracy (usually stated at 10^{-3} – 10^{-4}). It is unmatched by any other technique that could provide direct reference measurement for comparison. Modelling and metrology of TPP

could be used to imply certain metrological parameters of the phantom, and while this approach is far from being rigorous or standardized, it might be the only option to provide the expected 3D RI for evaluation.

4. Discussion and conclusions

In rapidly progressing field of QPI end-to-end approach to metrology is desired. In such approach a calibration sample is measured and analyzed using the same presets and protocol as for the biological specimen, and the results are expressed as key biophysical parameters of the sample. The measurement system and necessary data processing can be treated as a black box, since the comparison happens between the known input (phantom standard) and

measured set of quantities that the sample has been calibrated for. It greatly decreases barrier to entry for comprehensive metrological evaluation of the QPI systems, since the detailed knowledge and analytical models of the device are not required. Instead, the challenges are transferred over to the phantom fabrication and characterization, since standards have to be developed for a particular application in mind and each particular cell morphology or culture behaviour warrants its own phantom.

End-to-end approach, however, is not well compatible with the current national level standard certification protocols. At the Central Office of Measures in Poland, the one-dimensional and two-dimensional phantoms presented in this work could be measured using MII-4 microscope interferometer ((240×160×1) μm measurement range, expanded uncertainty $U = 11$ nm, relative uncertainty $u_r \approx 1\%$), a contact profilometer ((60×100×2) mm, $U = 30$ nm ÷ 59 nm, $u_r \approx 0.3\%$), and the Nanomeasuring Machine (NMM-1) equipped with an atomic force microscope (AFM) and white-light interferometer module. Depending on the needs and consequently the system used for measurements, one can obtain a different measurement range and expected measurement uncertainty. In the case of the most accurate settings of the NMM-1, the measurement range with equipped AFM head is (25×25×5) μm, the resolution of the measurement system is 0.1 nm and the expected measurement uncertainty is at the level of single nanometers ($u_r \approx 0.1\%$). Measurements of RI standards are performed by the precise geometric measurements laboratory of the Central Office of Measures using a goniometer-spectrometer II UV-VIS-IR. It is equipped with two equilateral prisms and two recess prisms, and the RI is determined by the goniometric method based on measurements of the prism's angle of refraction and the angle of the smallest deviation. Calibration is performed in the visible light range (405 ÷ 656) nm. This setup is used to determine the refractive index of solids and liquids refractometric standards in the range of 1.300000 ÷ 1.900000 with expanded uncertainty ($k = 2$) of the order of 3×10^{-6} ($u_r \approx 10^{-4}\%$). While these systems are capable of calibration of quantities in the appropriate range as indicated in Tab. 2, both geometry and RI have to be evaluated separately and require different forms of samples. Therefore this approach is more appropriate for the evaluation of the fabrication technique, but even then the fabrication parameters can change and the accuracy is sample-dependent. For direct calibration even two-dimensional phantoms there is a need for aerial profilometry with high spatial resolution and height uncertainty defined in relation to spatial frequency of the sample, as well as accurate measurements of the RI in the micro-scale. Bridging the gap between calibrated scalar measurements and full-field or

even volumetric data holds the key to make the best out of the wealth of information provided by the QPI.

Therefore, it is envisioned that 3D-printed microphantoms as described here are going to be widely utilized to support the development and validation of measurement instruments not limited to QPI. Along with the advancements in the fabrication capabilities, more and more materials including composites will enable phantoms for various modalities (contrasts) and with advantageous properties (e.g. 3D-printed glass [23] for stability and environmental resiliency). Optical instruments working in transmission are generally sensitive to the RI distribution within the sample, even if it is not the quantity that they ultimately measure. Therefore most such systems could utilize presented phantoms for investigation and minimization of sample-induced aberrations caused by the RI inhomogeneities. Lastly, phantom generation and fabrication can be automated in order to create large experimental datasets, which are pivotal for training and validation of machine learning approaches to imaging and detection in biomedicine and industry.

Acknowledgments

This work has received funding from Polish Ministry of Education and Science (Polish Metrology, PM/SP/0079/2021/1) and Warsaw University of Technology under the program Excellence Initiative: Research University (IDUB).

Author Contribution MZ: Conceptualization, methodology, visualization, writing - original draft; **DC:** Writing - review & editing; **MK:** Conceptualization, writing - review & editing, supervision, funding acquisition.

Conflict of interest The authors declare no conflicts of interest.

References

- [1] Popescu G., Quantitative phase imaging of cells and tissues (New York: McGraw-Hill, 2011).
- [2] Balasubramani V., et al. Roadmap on Digital Holography-Based Quantitative Phase Imaging. *Journal of Imaging* 7, 252 (2021). URL <https://www.mdpi.com/2313-433X/7/12/252>
- [3] Kemper B. & von Bally G., Digital holographic microscopy for live cell applications and technical inspection. *Applied Optics* 47, A52 (2008). URL <http://dx.doi.org/10.1364/AO.47.000A52>.
- [4] Park Y., Depeursinge C. & Popescu G., Quantitative phase imaging in biomedicine. *Nature Photonics* 12, 578–589 (2018).

- [5] Astratov V. N. et al., Roadmap on label-free super-resolution imaging. *Laser & Photonics Reviews* 17, 2200029 (2023).
- [6] Nguyen T. L. et al., Quantitative phase imaging: recent advances and expanding potential in biomedicine. *ACS Nano* 16, 11516–11544 (2022).
- [7] Leslie K. A. et al., Reconstituting donor t cells increase their biomass following hematopoietic stem cell transplantation. *The Analyst* 143, 2479–2485 (2018). URL <http://dx.doi.org/10.1039/C8AN00148K>.
- [8] Kandel M. E. et al., Multiscale assay of unlabeled neurite dynamics using phase imaging with computational specificity. *ACS Sensors* 6, 1864–1874 (2021). URL <http://dx.doi.org/10.1021/acssensors.1c00100>.
- [9] Liu Y. & Uttam S., Perspective on quantitative phase imaging to improve precision cancer medicine. *Journal of Biomedical Optics* 29, 1–22 (2024). URL <https://www.spiedigitallibrary.org/journals/journal-of-biomedical-optics/volume-29/issue-S2/S22705/Perspective-on-quantitative-phase-imaging-to-improve-precision-cancer-medicine/10.1117/1.JBO.29.S2.S22705.full>.
- [10] Haeberlé O., Belkebir K., Giovaninni H. & Sentenac A., Tomographic diffractive microscopy: Basics, techniques and perspectives. *Journal of Modern Optics* 57, 686–699 (2010).
- [11] Verrier N., Debailleul M. & Haeberlé O., Recent advances and current trends in transmission tomographic diffraction microscopy. *Sensors* 24, 1594 (2024).
- [12] Chowdhury S. et al., High-resolution 3D refractive index microscopy of multiple scattering samples from intensity images. *Optica* 6, 1211 (2019). URL <https://www.osapublishing.org/abstract.cfm?URI=optica-6-9-1211>.
- [13] Yasuhiko O., Takeuchi K., Yamada H. & Ueda Y., Multiple-scattering suppressive refractive index tomography for the label-free quantitative assessment of multicellular spheroids. *Biomedical Optics Express* 13, 962 (2022). URL <http://dx.doi.org/10.1364/BOE.446622>.
- [14] Tong Z. et al., Three-dimensional refractive index microscopy based on the multilayer propagation model with obliquity factor correction. *Optics and Lasers in Engineering* 174, 107966 (2024). URL <http://dx.doi.org/10.1016/j.optlaseng.2023.107966>.
- [15] Kamilov U. S. et al., Learning approach to optical tomography. *Optica* 2, 517 (2015). URL <http://dx.doi.org/10.1364/OPTICA.2.000517>.
- [16] Lim J. & Psaltis D., Maxwellnet: Physics-driven deep neural network training based on maxwell's equations. *APL Photonics* 7 (2022). URL <http://dx.doi.org/10.1063/5.0071616>.
- [17] Yang D. et al., Refractive index tomography with a physics-based optical neural network. *Biomedical Optics Express* 14, 5886 (2023). URL <http://dx.doi.org/10.1364/BOE.504242>.
- [18] Hugonnet H. et al., histopathologytion of Multiscale label-free volumetric holographic thick-tissue slides with subcellular resolution. *Advanced Photonics* 3, 1–8 (2021). URL <https://www.spiedigitallibrary.org/journals/advanced-photonics/volume-3/issue-02/026004/Multiscale-label-free-volumetric-holographic-histopathology-of-thick-tissue-slides/10.1117/1.AP.3.2.026004.full>.
- [19] Lee M. J. et al., Long-term three-dimensional high-resolution imaging of live unlabeled small intestinal organoids via low-coherence holotomography. *Experimental & Molecular Medicine* (2024). URL <http://dx.doi.org/10.1038/s12276-024-01312-0>.
- [20] Li J. et al., Transport of intensity diffraction tomography with non-interferometric synthetic aperture for three-dimensional label-free microscopy. *Light: Science & Applications* 11, 154 (2022). URL <https://www.nature.com/articles/s41377-022-00815-7>.
- [21] Ziemczonok M., Kuś A. & Kujawińska M., Optical diffraction tomography meets metrology – Measurement accuracy on cellular and subcellular level. *Measurement* 195, 111106 (2022). URL <https://doi.org/10.1016/j.measurement.2022.111106> <https://linkinghub.elsevier.com/retrieve/pii/S0263224122003700>.
- [22] Ziemczonok M. & Kujawińska M., Multiscale and multipurpose phantoms for 2D/3D quantitative phase imaging. *Proc. SPIE* 1238908, 36–42 (2023).
- [23] Wang H. et al., Two-Photon Polymerization Lithography for Optics and Photonics: Fundamentals, Materials, Technologies, and Applications. *Advanced Functional Materials* 33

- (2023). URL <https://onlinelibrary.wiley.com/doi/10.1002/adfm.202214211>.
- [24] Liao C., Wuethrich A. & Trau M., A material odyssey for 3D nano/microstructures: two photon polymerization based nanolithography in bioapplications. *Applied Materials Today* 19, 100635 (2020). URL <https://doi.org/10.1016/j.apmt.2020.100635>
<https://linkinghub.elsevier.com/retrieve/pii/S2352940720300834>.
- [25] Guney M. G. & Fedder G. K., Estimation of line dimensions in 3D direct laser writing lithography. *Journal of Micromechanics and Microengineering* 26, 105011 (2016). URL <http://dx.doi.org/10.1088/0960-1317/26/10/105011>.
- [26] Žukauskas A. et al., Tuning the refractive index in 3D direct laser writing lithography: towards GRIN microoptics. *Laser & Photonics Reviews* 9, 706–712 (2015).
- [27] Gonzalez-Hernandez D. et al., Single-Step 3D Printing of Micro-Optics with Adjustable Refractive Index by Ultrafast Laser Nanolithography. *Advanced Optical Materials* 11, 1–7 (2023). URL <https://onlinelibrary.wiley.com/doi/10.1002/adom.202300258>.
- [28] Eifler M. et al., Comparison of material measures for areal surface topography measuring instrument calibration. *Surface Topography: Metrology and Properties* 8, 025019 (2020). URL <https://iopscience.iop.org/article/10.1088/2051-672X/ab92ae>.
- [29] Eifler M., Hering-Stratemeier J., von Freymann G. & Seewig J., Comprehensive profile and areal calibration by additively manufactured material measures. *Surface Topography: Metrology and Properties* 12, 015013 (2024). URL <http://dx.doi.org/10.1088/2051-672X/ad2985>.
- [30] Horstmeyer R., Heintzmann R., Popescu G., Waller L. & Yang C., Standardizing the resolution claims for coherent microscopy. *Nature Photonics* 10, 68–71 (2016). URL <http://dx.doi.org/10.1038/nphoton.2015.279>
<http://www.nature.com/articles/nphoton.2015.279>.
- [31] Godden, T. M., Muñoz-Piniella, A., Claverley, J. D., Yacoot, A. & Humphry, M. J. Phase calibration target for quantitative phase imaging with ptychography. *Optics Express* 24, 7679 (2016). URL <https://www.osapublishing.org/abstract.cfm?URI=oe-24-7-7679>
<https://opg.optica.org/abstract.cfm?URI=oe-24-7-7679>.
- [32] de Groot P. J., The instrument transfer function for optical measurements of surface topography. *Journal of Physics: Photonics* 3, 024004 (2021). URL <https://iopscience.iop.org/article/10.1088/2515-7647/abe3da>.
- [33] Desissaire S. et al., Bio-inspired 3D-printed phantom: Encoding cellular heterogeneity for characterization of quantitative phase imaging. *Measurement* 247, 116765 (2025). URL <https://linkinghub.elsevier.com/retrieve/pii/S0263224125001241>.
- [34] Krauze W. et al., 3D scattering microphantom sample to assess quantitative accuracy in tomographic phase microscopy techniques. *Scientific Reports* 12, 19586 (2022).